frontiers | Frontiers in Materials

TYPE Original Research
PUBLISHED 09 December 2022
DOI 10.3389/fmats.2022.1097547

OPEN ACCESS

EDITED BY
Jingjun Wu,
Zhejiang University, China

REVIEWED BY
Xiaozhen Zhang,
Jingdezhen Ceramic Institute, China
Shanwen Tao,
University of Warwick, United Kingdom

*CORRESPONDENCE
Kui Xie,
kxie@fjirsm.ac.cn

SPECIALTY SECTION
This article was submitted to Polymeric and Composite Materials, a section of the journal Frontiers in Materials

RECEIVED 14 November 2022
ACCEPTED 24 November 2022
PUBLISHED 09 December 2022

CITATION
Li X and Xie K (2022), Porous single-crystalline molybdenum nitride enhances electroreduction of nitrogen to ammonia.
Front. Mater. 9:1097547.
doi: 10.3389/fmats.2022.1097547

Porous single-crystalline molybdenum nitride enhances electroreduction of nitrogen to ammonia

Xue Li[1,2] and Kui Xie[2,3]*

[1]College of Chemistry and Materials Science, Fujian Normal University, Fuzhou, China, [2]Key Laboratory of Design and Assembly of Functional Nanostructures, Fujian Institute of Research on the Structure of Matter, Chinese Academy of Sciences, Fuzhou, China, [3]Advanced Energy Science and Technology Guangdong Laboratory, Huizhou, China

The industrial ammonia synthesis reaction has the disadvantage of large energy consumption; thus, the electrochemical reduction method of ammonia synthesis characterized by its clean nature and environmental protectiveness has received extensive attention. Molybdenum nitride is a commonly used electrocatalyst for ammonia synthesis, and its Faraday efficiency is low, which may be due to many internal grain boundaries and few active sites. In this work, we grow microscale porous Mo_2N single crystals and polycrystalline Mo_2N from non-porous MoO_3 single crystals. Porous molybdenum nitride materials facilitate charge transport in grain boundaries due to their single-crystal nature and enhance the catalytic properties of ammonia synthesis reactions. Compared with polycrystalline Mo_2N, the porous Mo_2N single crystal shows better performance, with a high NH_4^+ yield of 272.56 μg h^{-1} mg^{-1} and a Faradaic efficiency of 7.3%. In addition, the porous Mo_2N single crystal exhibits superior long-term stability with little attenuation after 16 h electrolysis reaction. It provides a new method for the catalyst of ammonia synthesis.

KEYWORDS

porous single crystal, molybdenum nitride, electrochemical reactions, ammonia, hydrothermal method

Introduction

Shortage of ammonia (NH_3), which is used as the raw material for chemical fertilizer, chemical pharmaceuticals, and zero-carbon emission fuel, has become an urgent energy problem with the continuous growth of the population. Fixing N_2 in the atmosphere to NH_3 is an important method to realize nitrogen storage and the conversion of Earth's nitrogen cycle (Service, 2014; Brown et al., 2016). Up to now, the Haber–Bosch method ($N_2 + 3H_2 \rightarrow 2NH_3$) has been used to synthesize NH_3 in the industry, which works at high temperatures and pressure with high energy consumption (Van Der Ham et al., 2014). Most raw materials of hydrogen and energy consumption are obtained through the steam reformation of fossil fuels, while a large amount of CO_2 is also produced (Kyriakou et al.,

2020). Therefore, the more economical, environmental, and sustainable method of producing NH_3 is in great demand.

Electrochemical reduction is a prospective method for artificial nitrogen fixation (Amar et al., 2011; Costentin et al., 2013; She et al., 2017; Guo et al., 2018). However, the N_2 reduction reaction (NRR) requires breaking the inert molecular structure of N_2, which requires sufficient energy to break the N≡N bond (~941 kJ mol^{-1}) (Han et al., 2021). Noble metal catalysts (Ru, Au, Ag, and Rh) have shown to have superior NRR activity, but the high cost and rareness limit their commercial applications (Aioub et al., 2017; Bao et al., 2017; Nazemi et al., 2018; Liu et al., 2019; Tao et al., 2019). The search for inexpensive, earth-abundant materials with high activity and excellent stability has recently attracted significant research interest and has become an important pursuit toward ammonia economy. In recent years, transition metal has attracted extensive attention as NRR catalysts because of their high activity, abundant reserves, and low price. It has been reported that molybdenum-based catalysts have been designed and applied to artificial nitrogen fixation (Banerjee et al., 2015; Sun et al., 2017; Wickramasinghe et al., 2017; Yang et al., 2017; Han et al., 2018; Li et al., 2019; Ou et al., 2019). Molybdenum nitride has attracted much attention due to its platinum-like properties. Specifically, Mo_2N is a typical interstitial compound in which the metal atoms express a tight stacking pattern to stabilize the lattice structure, where the top element is mainly a metal atom on the surface. The nearest metal ions with short distances will provide the possibility to form metallic bonds to facilitate electron transport in the connected channels. MoN and Mo_2N nanosheets also have an electrocatalytic activity of N_2 reduction, with the FE of 1.15% and 4.5%, respectively (Ren et al., 2018; Zhang et al., 2018). Although molybdenum-based catalysts have excellent performance, they still suffer from weak FE efficiency. Thus, it is attractive to search for new Mo-based catalysts with enhanced FE performance.

In catalytic and electrocatalytic systems, uniform dispersion of active sites on the surface of porous structures ensures the high activity of porous materials (Zhang et al., 2021; Lu et al., 2022). Single crystals with almost no grain boundary reduce the resistance of charge transmission between grain boundaries. Therefore, porous single crystals with anisotropy and a long-range structural order and structural coherence combined with a large specific surface area provide unsaturated nitrogen coordination on the surface of metal nitride, and its internal structures exhibit regularity and periodicity in three-dimensional space. Due to the porous single-crystal structure, the electrocatalytic properties are also improved (Wu et al., 2019; Zhang et al., 2019; Lin et al., 2020, 2022; Xiao and Xie, 2022). Different from the conventionally used nano-catalyst materials such as nanosheets or nanorods, which are smooth in surface and poor in single crystallinity, porous single crystals have a large amount of nanopores and good crystallinity which increase the active site and improve the stability during the reaction, thus improving the catalytic performance of the catalyst.

In this paper, we prepare the micron-scale porous Mo_2N single crystal (PSC Mo_2N) and polycrystalline Mo_2N (PPC Mo_2N) cubes by the lattice reconstruction strategy and investigate their catalytic performance in the electrocatalytic reduction of N_2 to NH_3. PSC Mo_2N can provide a large surface area for chemical adsorption, and the internal interconnected pores and channels are conducive to the diffusion of ions in the electrolyte. PSC Mo_2N exhibits ultra-high yield of NH_3 and FE, which greatly enhances the catalytic performance of NRR.

Materials and methods

Syntheses of a porous Mo_2N single crystal

The MoO_3-PEG precursor is obtained by the hydrothermal method. MoO_3-PEG is kept at 300°C for 5 h in air and cooled down naturally to obtain MoO_3. PSC Mo_2N is obtained in a tube furnace at 650°C for 10 h at a pressure of 50–200 Torr with 100 sccm NH_3 gas flow rates. Similarly, irregular porous polycrystalline molybdenum nitride (PPC Mo_2N) is obtained by direct treatment of MoO_3 single crystals in a tube furnace at atmospheric pressure with NH_3 gas at 50–200 sccm for 10 h at 650°C. All reagents are used without any purification.

Characterizations

An X-ray diffractometer (XRD, Bruker D8-Advance) is used to characterize the phase composition of synthetic materials and determine the crystal face and crystal orientation. The surface morphologies of MoO_3 and Mo_2N are observed by field emission scanning electron microscopy (FE-SEM, SU8010) with 10 kV accelerating voltage. The Tecnai F30 microscope with 200 kV accelerating voltage is tested for transmission electron microscopy (TEM) and selected area electron diffraction (SAED). TEM (FEI Titan 3G2 60-300) is corrected by the spherical aberration method at 300 kV accelerating voltage, and the atomic information and crystal structure of the material are characterized. The Brunauer–Emmett–Teller (BET) tests are performed by an automatic specific surface and micropore analyzer (Tristar II 3020). X-ray photoelectron spectroscopy (XPS, Escalab 250Xi) tests the binding energy of the crystals. The product NH_4^+ is quantified by cation chromatography (IC 1826 Qingdao, Shunyuhengping).

Preparation of electrodes

The catalyst samples are mixed in ethanol and Nafion solution and sonicated for 30 min to prepare a homogeneous suspension of the catalyst. The prepared suspension is then

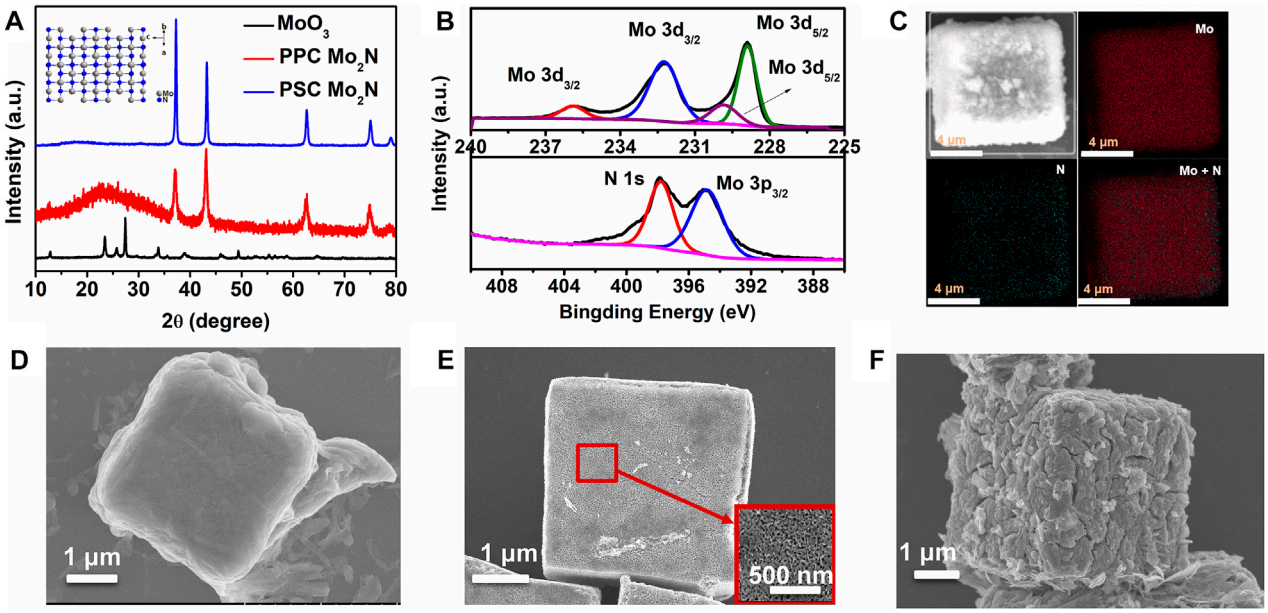

FIGURE 1
(A) XRD patterns of MoO_3 microcubes, Mo_2N porous single crystals, and polycrystalline microcubes. The inset in **(A)** is the crystal structure of Mo_2N. **(B)** Mo_2N of XPS spectra. **(C)** EDX elemental mapping of Mo and N in Mo_2N microcubes. SEM of **(D)** MoO_3, **(E)** PSC Mo_2N, and **(F)** PPC Mo_2N. The inserted image of **(E)** is a partial amplification of the SEM image.

dropped on a piece of carbon paper (CP) to obtain a 5 mg cm^{-2} sample, which is dried naturally at room temperature to acquire the working electrode.

Electrochemical measurements

Electrochemical data are obtained by testing with the three-electrode system (Zahner, Ennium) of the chemical workstation. Electrocatalytic NRR is a typical hydrogen reduction process. The study is performed in a closed H-shaped vessel with the middle section separated by a Nafion 117 membrane. The electrochemical workstation is operated at room temperature with Mo_2N (Mo_2N/CP) as the working electrode, carbon paper as the substrate, a graphite electrode as the counter electrode, and a saturated Ag/AgCl electrode as the reference electrode, as well as 0.1 M HCl solution as the electrolyte. With the help of N_2 and H^+, NH_3 is obtained at the cathode. Two-compartment batteries can avoid NH_3 oxidation in the anode. In particular, the resistance of the Nafion 117 membrane is negligible. The Nafion 117 membrane only transmits H^+, which can limit the diffusion of NH_3 to the anode. The potential is calibrated and converted into a reversible hydrogen electrode (RHE) using the following formulas (Ren et al., 2018).

$$E\,(RHE) = E\,(Ag/AgCl) + 0.059\,pH + 0.197\,V, \quad (1)$$

where E (RHE) is the corrected potential (V) versus RHE, E (Ag/AgCl) is the experimental test potential with Ag/AgCl as the reference electrode, and 0.197 V is the potential at room temperature at the standard electrode for the Ag/AgCl electrode.

We simultaneously collected products under different potential conditions ranging from −0.3 to −0.8 V for 2 h. The concentration of NH_4^+ is tested by cation chromatography. The generation rate of NH_4^+ and the Faradaic efficiency (FE) of the current are calculated by the formula and plotted. Among them, the calculation of the NH_3 generation rate and FE is as follows:

$$\text{Ammonia formation rate}\,(ug\,h^{-1}\,mg^{-1}) = [NH_4^+] \times V \div (m \times t), \quad (2)$$

$$FE\,(\%) = 3 \times F \times [NH_4^+] \times V \div (17 \times Q), \quad (3)$$

where $[NH_4^+]$ is the result of measuring the NH_4^+ concentration, V is the volume of the electrolyte at the cathode, m is the loaded mass of the catalyst, t is the time of potential application, Q is the Coulomb volume through the electrode, and F is the Faraday constant.

Linear sweep voltammetry (LSV) is applied to estimate the catalytic performance and stability of OER at 10 mV s^{-1} in 0.1 M HCl. We measure a three-electrode cell system whose electrochemical impedance spectrum (EIS) is measured between 0.1 Hz and 2 MHz at 0.1 M hydrochloric acid and 5 mV AC potential. The current density curve is obtained from the variation of Mo_2N of NRR with time at various potentials in 0.1 M HCl.

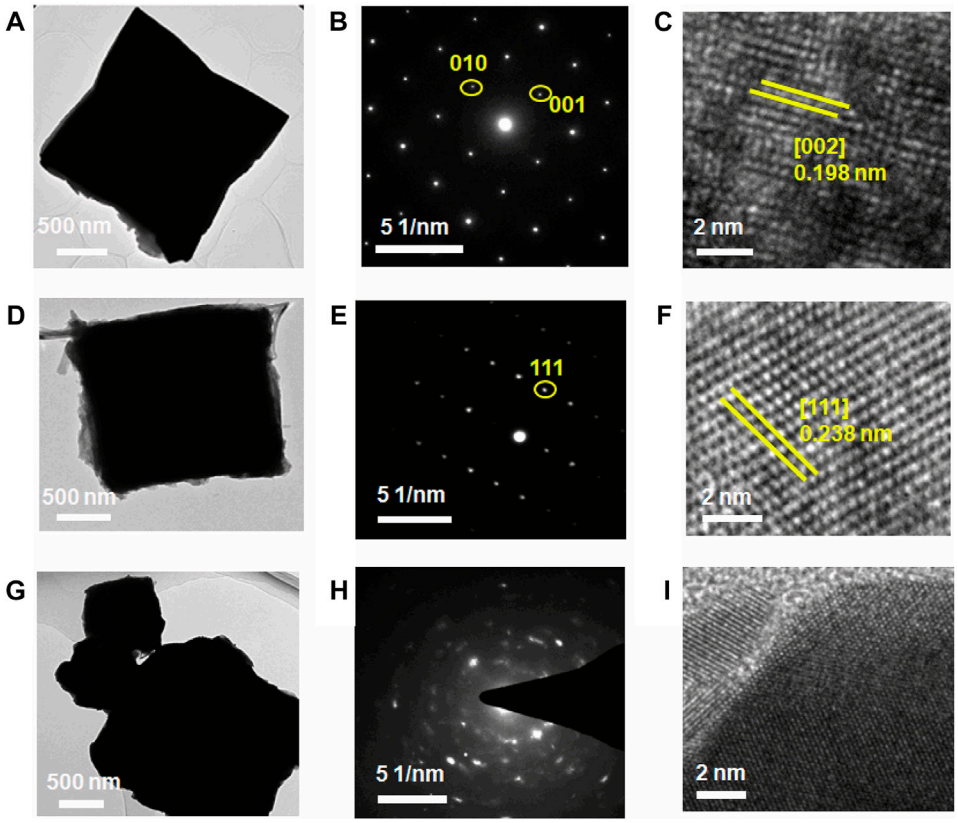

FIGURE 2
TEM image, SAED pattern, and HRTEM image of the material. **(A–C)** MoO_3 single-crystal microcube, **(D–F)** PSC Mo_2N microcube, and **(G–I)** PPC Mo_2N.

Results and discussion

Figure 1A shows the XRD patterns of MoO_3, PSC Mo_2N, and PPC Mo_2N. The XRD patterns of MoO_3 and Mo_2N single crystals conform to the JCPDS standard cards 75-0512 and 75-1150, respectively. The diffraction peaks are sharp and narrow, indicating that molybdenum nitride has excellent crystallinity. From a polycrystalline versus a single crystal perspective, molybdenum nitride single crystals tend to be [111] oriented. The inset in Figure 1A is ball-and-stick model of the crystal structure of Mo_2N. Supplementary Figure S1 illustrates the growth mechanism for obtaining micron-scale metal nitride cubes from metal oxides. When the intrinsic oxygen atoms in the MoO_3 lattice are heated in an ammonia atmosphere, the oxygen atoms gradually leave the intrinsic position in the lattice and slowly disappear. The nitrogen atom in ammonia gradually enters the position before the oxygen atom. Due to the different sizes of oxygen and nitrogen atoms, the lattice configuration also changes, and then, the molybdenum nitride skeleton is gradually formed. By changing the ammonia flow rate and pressure, the molybdenum nitride lattice is reconstructed to form a porous Mo_2N cube.

To explore the relationship between the structure and properties of porous single-crystal molybdenum nitride, we perform XPS tests. The test results are shown in Figure 1B; the results specifically show that the characteristic peaks at 229.8 and 232.3 eV are caused by Mo $3d_{5/2}$ and Mo $3d_{3/2}$ (Ozkan et al., 1997; Afanasiev, 2002; Liu et al., 2013). In addition, the combining energies at 228.9 and 235.9 eV are consistent with $Mo^{\delta+}$ and Mo^{6+}, respectively, which is ascribed to the surface oxidation of Mo_2N (Yoon et al., 2012). The peak at 397.81 eV is the N 1 s of Mo_2N, while the peak value of 394.77 eV corresponds to the shoulder of $Mo3p_{3/2}$ with Mo_2N, indicating the presence of Mo–N bonds (Ozkan et al., 1997; Afanasiev, 2002; Yoon et al., 2012; Liu et al., 2013). To further confirm the presence of chemical elements in Mo_2N, energy dispersive X-ray (EDX) and its mapping are used for further identification (Figure 1C). The results indicate that only two chemical elements (Mo and N) can be detected in the final product Mo_2N, and no other impurity phases are observed. Moreover, the chemical elements Mo and N are uniformly

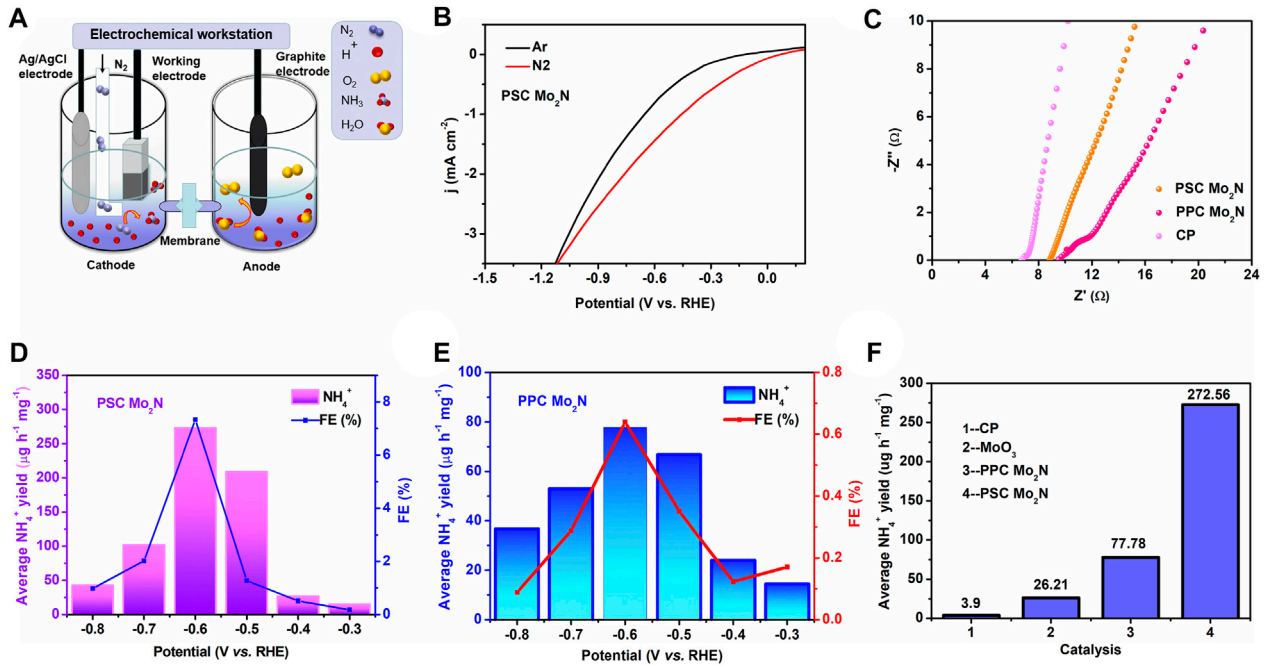

FIGURE 3
(A) Schematic diagram of electrocatalytic NRR. **(B)** LSV curve of PSC Mo_2N electrocatalytic NRR in a saturated electrolyte of N_2 (red line) and Ar (black line). **(C)** Nyquist plots of CP, PSC Mo_2N, and PPC Mo_2N catalysts in 0.1 M HCl solution. The yields of NH_4^+ and FEs at different potentials of **(D)** PSC Mo_2N and **(E)** PPC Mo_2N. **(F)** Yields of NH_4^+ in different catalysts under the same environmental conditions at −0.6 V vs. RHE.

distributed in the sample, which confirms well the complete transformation process of the non-porous MoO_3 single crystal.

We observe the changes in the microscopic morphology of the crystals during the growth and preparation processes by SEM, and Figure 1D shows the MoO_3 cubes of about 3–10 μm obtained after calcination of the precursor MoO_3-PEG. Figures 1E,F display the microcube scanning diagram of PSC Mo_2N and PPC Mo_2N formed by ammoniation of MoO_3, which have the same morphology before and after calcination from the microscopic scale. In addition, Figure 1E reveals the magnified morphology, and it can be seen that the pore channels are uniformly connected roughly around 50 nm, while the polycrystalline surface is in a sintered state with some cracks. Therefore, we speculate that the specific surface area of single crystals should be larger than that of polycrystals. We use a lattice reconstruction strategy to grow porous molybdenum nitride from non-porous molybdenum nitride, whose BET results (Supplementary Figure S2) indicate that the BET-specific surface areas of PSC Mo_2N and PPC Mo_2N are 14.347 and 7.676 $m^2 g^{-1}$, respectively. The larger specific surface area has more active sites, which is consistent with our subsequent test results (PSC Mo_2N > PPC Mo_2N).

For the purpose of obtaining further information about the microstructure and crystal orientation of the synthesized material, TEM and HRTEM are used for characterization and analysis. Figure 2A demonstrates that the precursor MoO_3 has good single crystallinity, where SAED (Figure 2B) corresponds to the (002) plane of MoO_3. HRTEM (Figure 2C) indicates a crystal surface spacing of 0.198 nm that corresponds to the (002) face of MoO_3, which is in agreement with both results. Mo_2N retains the morphology and structure of the precursor, irrespective of it being a single crystal (Figures 1E, 2D) or polycrystalline (Figures 1F, 2G). Figure 2F taken with HRTEM from a single Mo_2N cube (Figure 2I) reveals highly resolved lattice stripes between the crystal planes with a crystalline spacing of 0.238 nm associated with the (111) plane of Mo_2N, which is consistent with SAED (Figure 2E). This further establishes that the sample has a defined crystal orientation. However, in Figures 2H,I, the SAED is tending to a ring-like pattern, and there are no distinct and regular lattice stripes, which suggests that the sample is polycrystalline.

NRR is a prototypical reduction process by hydrogenation. As shown in Figure 3A, N_2 bubbles to the cathode surface, and H^+ can be transferred through the electrolyte of 0.1 M HCl to react with the cathode Mo_2N to form NH_3. At first, we test the electrochemical performance of the sample and the catalytic activity of N_2. The LSV curves for the reduction reaction (NRR) are obtained by saturating with N_2 and Ar in 0.1 M HCl electrolyte (Figure 3B), and it is clear that the current density of N_2 increases slightly compared to Ar in the saturated

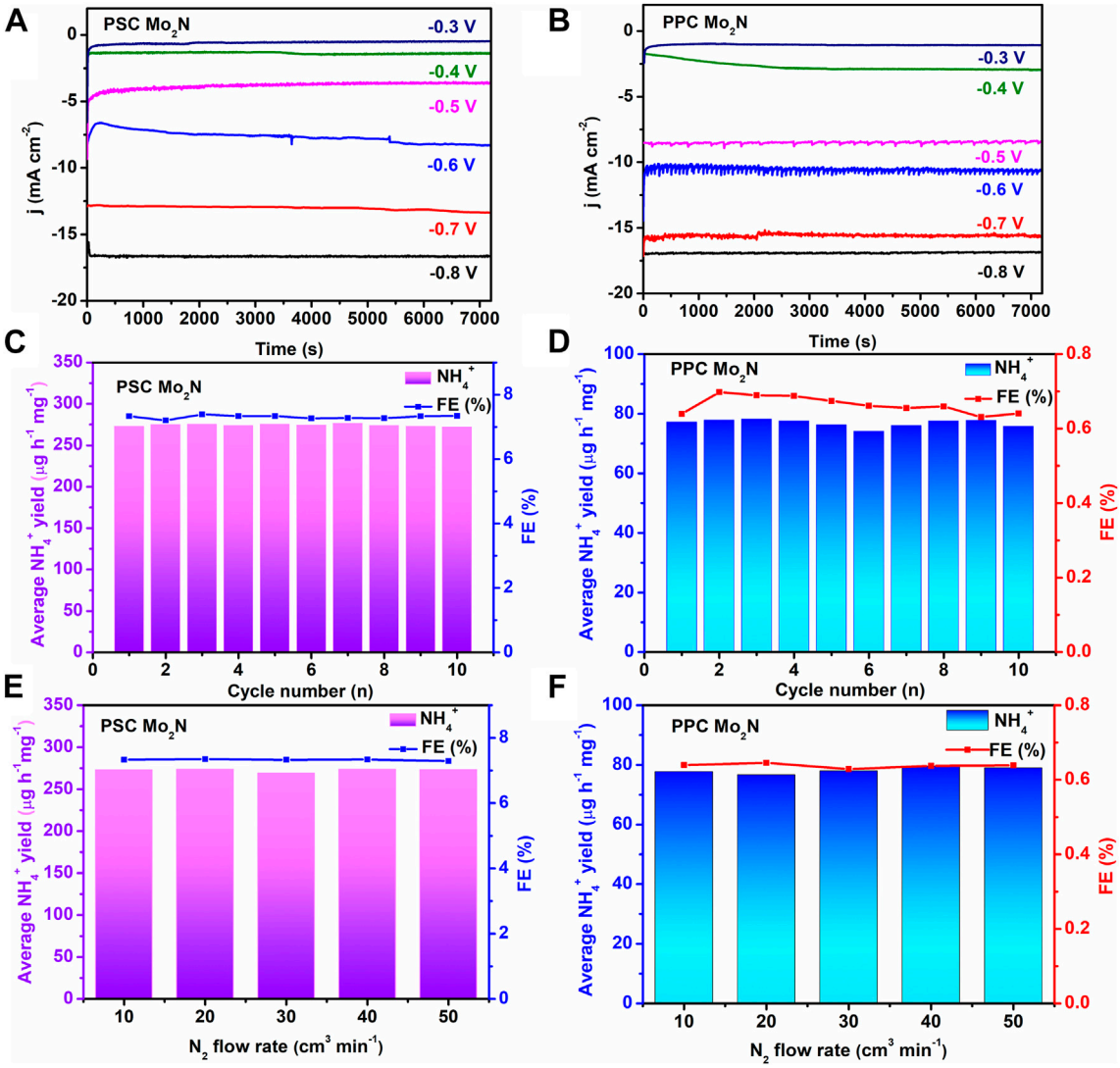

FIGURE 4
Current density curves of **(A)** PSC Mo_2N and **(B)** PPC Mo_2N of NRR with time at different voltages in 0.1 M HCl. The yields of NH_4^+ and FEs, 10 of **(C)** PSC Mo_2N and **(D)** PPC Mo_2N at −0.6 V vs. RHE potential during the cycle test. The yields of NH_4^+ and FEs of **(E)** PSC Mo_2N and **(F)** PPC Mo_2N catalysts at different N_2 flow rates.

electrolyte, which indicates the potential NRR activity of PSC Mo_2N. Apart from that, the AC impedance method is used to verify the electron transfer resistance of molybdenum nitride by fitting the EIS data on the sample to an equivalent circuit. The Nyquist curve (Figure 3C) shows that PSC Mo_2N has a smaller resistance than PPC Mo_2N and therefore has a higher current for the same voltage conditions applied. This indicates that the porous single crystal is conducive to carrier migration, which has better catalytic properties. All these results clearly indicate that the porous Mo_2N single crystals are more effective as electrocatalysts than polycrystals.

In the next step, we collect the products at different voltages at the same time and analyze their contents by cation chromatography. The results are shown in Figures 3D,E, which exhibit the NH_4^+ yields and FEs of PSC Mo_2N and PPC Mo_2N at different voltages. Among them, the catalytic effect of the catalysts is best at −0.6 V, when the NH_4^+ production rate of PPC Mo_2N is 77.78 μg h^{-1} mg^{-1} and the FE reached 0.6%, while the NH_4^+ production rate of PSC Mo_2N reached 272.56 μg h^{-1} mg^{-1} and the FE reached 7.3%. Obviously, PSC Mo_2N implies extremely high catalytic activity compared to PPC Mo_2N. The NH_4^+ yield and FE content increase with the increase in negative voltage; however, the yield of NH_4^+ and FE decreases significantly when it passes −0.6 V vs. RHE. It is possible that the hydrogen evolution reaction (HER) competes fiercely at the Mo_2N electrode to preferentially occupy the active

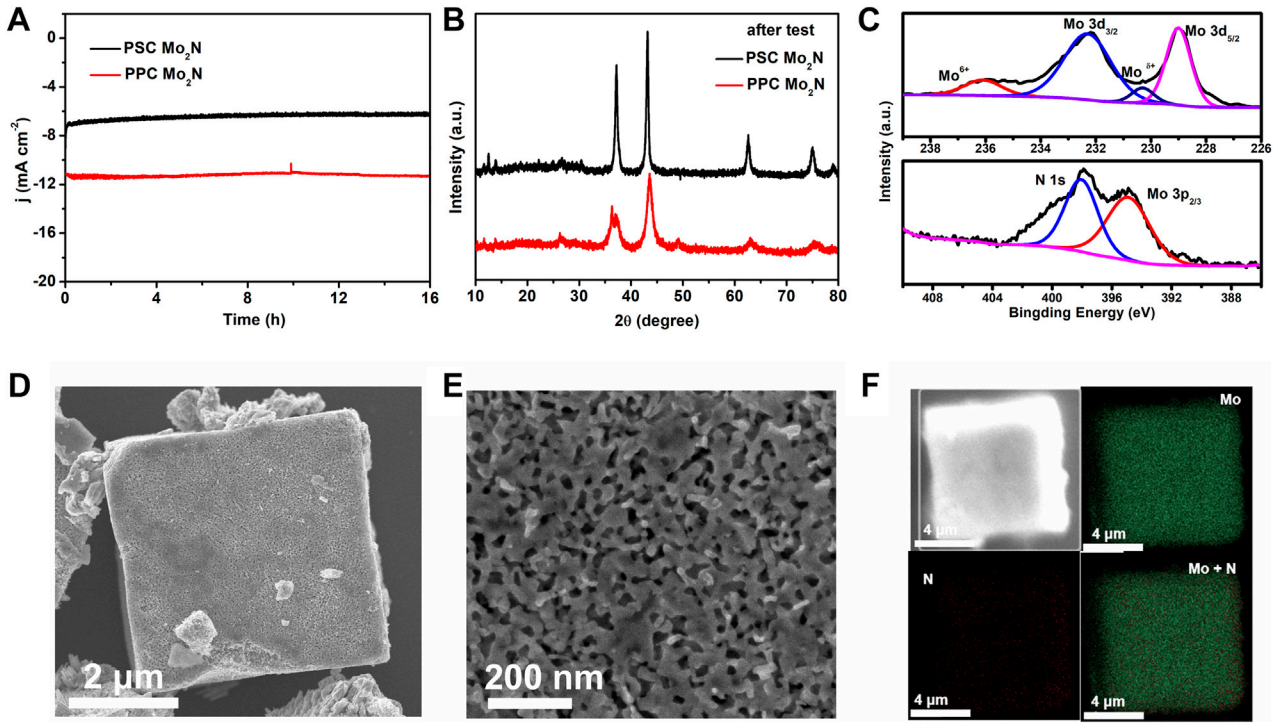

FIGURE 5
(A) Timing ampere curve of PSC Mo_2N and PPC Mo_2N electrolysis for 16 h at a potential of −0.6 V vs. RHE. **(B)** XRD of PSC Mo_2N and PPC Mo_2N after a long-term reaction. **(C)** Mo_2N of the XPS energy spectrum after a long-term reaction. **(D)** SEM images of different magnifications after the reaction. **(E)** Magnified view of SEM of PSC Mo_2N. **(F)** EDX elemental mapping of Mo and N in Mo_2N microcubes.

site with a large amount of free H and limit the effective trapping of N_2, hindering the forward progress of the NRR reaction. Compared with other water-based catalysts, PSC Mo_2N has higher ammonia yield and FE. The specific performance of other catalysts is shown in Supplementary Table S1.

The effect of other impurities in the experiments is excluded by conducting control experiments on the precursor MoO_3 and carbon paper on the results. The results demonstrate that the NRR rate of Mo_2N in Figure 3F is much higher than that of the MoO_3 single crystal (26.21 $\mu g\ h^{-1}\ mg^{-1}$), which implies that N plays an important role in the NRR and excludes the influence of surface oxidation on this reaction. At the same time, the bare CP shows weak NH_4^+ production, which has been subtracted from the starting data to reduce the experimental error. PSC Mo_2N and PPC Mo_2N have similar morphology and dimensions, but they have different specific surface areas, pore size, and lattice arrangement, leading to different ammonia yields of both. This suggests porous single crystals with large specific surface area and lattice continuity can reduce the energy loss of electron transfer between crystals, which results in higher catalytic activity. Therefore, PSC Mo2N exhibits excellent catalytic performance, which is consistent with the experimental results.

Durability is an important credential for assessing NRR response. Figures 4A,B indicate that the relative current density of PSC Mo_2N and PPC Mo_2N catalysts reduced to ammonia at different potentials respectively is stable, which shows the excellent durability of catalysts. Moreover, as the cathodic potential increases, the current density slightly decreases and the HER process is enhanced, inhibiting the NRR reaction, which is also consistent with the decrease of NH_4^+ production and FE. To further evaluate the stability of this catalytic process, we test the samples for 10 cycles at −0.6 V (Figures 4C,D), and the NH_4^+ production rate and FEs have no significant changes, indicating that they have good stability for NRR. In addition, the effect of a different N_2 flow rate on the product is also tested in this electrocatalytic process. As shown in Figures 4E,F, the approximately constant yields of NH_4^+ and FEs demonstrate that the N_2 diffusion rate has no obvious effect on the reaction, which ruled out the effect of the inlet concentration on this reaction. We perform some controlled experiments to verify the reliability of Mo_2N/CP for the electrochemical reduction of N_2 to NH_3. N_2 is led into the electrochemical reaction cell under open-circuit conditions, and saturated-Ar and saturated-N_2 gas flows are introduced separately for 2 h at −0.6 V vs. RHE, respectively. In summary, the influence of the external environment on the reaction during the experiment is excluded, indicating that the obtained NH_3 is derived from Mo_2N/CP.

We test the long-term electrolysis process, as shown in Figure 5A, and the current density electrochemical NRR process hardly changes significantly within 16 h, indicating the excellent performance of the Mo_2N catalyst. We perform a series of characterizations on the tested PSC Mo_2N such as XRD (Figure 5B), XPS (Figure 5C), SEM (Figures 5D,E), EDX (Supplementary Figure S4), and Mapping (Figure 5F). The test results clearly show that the phase composition, valence state, and elemental distribution of the catalyst itself have not changed significantly compared with those before the reaction, indicating that no other impurity phases are generated in the catalyst during the reaction. Further from the microscopic scale, PSC Mo_2N is able to maintain its initial composition and original cubic morphology after electrolysis, which also proves that the catalytic process is reproducibly cyclable and stable.

The aforementioned results and previous literature reports confirm that the possible NRR mechanism of Mo_2N can be described by the Mars–van Krevelen (MvK) process (Supplementary Figure S5) (Abghoui et al., 2016; Yang et al., 2017; Ren et al., 2018; Jin et al., 2019). First, H^+ is adsorbed on the N atoms on the surface of Mo_2N. Second, N vacancies appear on the catalyst face due to the departure of NH_3 molecules. Then, N_2 molecules occupy the vacancies, attracting H^+ to approach. Finally, NH_3 is released from the catalyst surface, and the Mo_2N catalyst returned to its original state. A steady stream of hydrogen ions in the electrolyte promotes the cyclic reaction. In the process of reaction, the porous structure increases the reaction area of the N atom and the active site of the reaction. Single-crystal materials are characterized by lattice continuity, so the migration process of N atoms is not blocked by grain boundaries. Compared with polycrystalline materials, it reduces the reaction kinetic energy of N atom migration, promotes the charge transfer of N atoms at the grain boundary, and accelerates the reaction rate. These results indicate that porous single-crystal molybdenum nitride has fine catalytic activity for the NRR reaction.

Conclusion

In summary, we prepare PSC Mo_2N and PPC Mo_2N. Among them, PSC Mo_2N reduces the charge transfer rate between grain boundaries and improves the rate and stability of the catalytic reaction due to its single-crystal nature. Compared with PPC Mo_2N, PSC Mo_2N exhibits excellent catalytic performance at −0.6 V vs. RHE, resulting in FE and yield of NH_4^+ up to 7.3% and 272.56 $\mu g\, h^{-1}\, mg^{-1}$. In addition, the reaction has superior recyclability and electrochemical durability, which maintains approximately constant yields of NH_3 and FE during 10 cycles and hardly weakens after 16 h long-term electrolysis. This work explores a novel avenue for the reasonable design and advancement of the molybdenum-based porous single crystal as the electrocatalysts of the artificial nitrogen fixation reaction.

Data availability statement

The original contributions presented in the study are included in the article/Supplementary Material; further inquiries can be directed to the corresponding author.

Author contributions

All authors listed have made a substantial, direct, and intellectual contribution to the work and approved it for publication. Investigation, data curation, software, formal analysis, visualization, writing—original draft: XL, Funding acquisition, project operation, writing review and editing: KX.

Funding

This work was supported by the National Key Research and Development Program of China (2021YFA1501500), the Natural Science Foundation of China (91845202), and the Strategic Priority Research Program of Chinese Academy of Sciences (XDB2000000).

Conflict of interest

Author KX was employed by the Advanced Energy Science and Technology Guangdong Laboratory.

The remaining author declares that the research was conducted in the absence of any commercial or financial relationships that could be construed as a potential conflict of interest.

Publisher's note

Supplementary material

The Supplementary Material for this article can be found online at the following link: https://www.frontiersin.org/articles/10.3389/fmats.2022.1097547/full#supplementary-material

References

Abghoui, Y., Garden, A. L., Howalt, J. G., Vegge, T., and Skúlason, E. (2016). Electroreduction of N_2 to ammonia at ambient conditions on mononitrides of Zr, Nb, Cr, and V: A dft guide for experiments. *ACS Catal.* 6, 635–646. doi:10.1021/acscatal.5b01918

Afanasiev, P. (2002). New single source route to the molybdenum nitride Mo_2N. *Inorg. Chem.* 41, 5317–5319. doi:10.1021/ic025564d

Aioub, M., Panikkanvalappil, S. R., and El-Sayed, M. A. (2017). Platinum-Coated gold nanorods: Efficient reactive oxygen scavengers that prevent oxidative damage toward healthy, untreated cells during plasmonic photothermal therapy. *ACS Nano* 11, 579–586. doi:10.1021/acsnano.6b06651

Amar, I. A., Lan, R., Petit, C. T. G., and Tao, S. (2011). Solid-state electrochemical synthesis of ammonia: A review. *J. Solid State Electrochem.* 15, 1845–1860. doi:10.1007/s10008-011-1376-x

Banerjee, A., Yuhas, B. D., Margulies, E. A., Zhang, Y., Shim, Y., Wasielewski, M. R., et al. (2015). Photochemical nitrogen conversion to ammonia in ambient conditions with femos-chalcogels. *J. Am. Chem. Soc.* 137, 2030–2034. doi:10.1021/ja512491v

Bao, D., Zhang, Q., Meng, F. L., Zhong, H. X., Shi, M. M., Zhang, Y., et al. (2017). Electrochemical reduction of N_2 under ambient conditions for artificial N2Fixation and renewable energy storage using N_2/NH_3 cycle. *Adv. Mat.* 29, 1604799. doi:10.1002/adma.201604799

Brown, K. A., Harris, D. F., Wilker, M. B., Rasmussen, A., Khadka, N., Hamby, H., et al. (2016). Light-driven dinitrogen reduction catalyzed by a CdS:nitrogenase MoFe protein biohybrid. *Science* 352, 448–450. doi:10.1126/science.aaf2091

Costentin, C., Robert, M., and Savéant, J. M. (2013). Catalysis of the electrochemical reduction of carbon dioxide. *Chem. Soc. Rev.* 42, 2423–2436. doi:10.1039/c2cs35360a

Guo, C., Ran, J., Vasileff, A., and Qiao, S. Z. (2018). Rational design of electrocatalysts and photo(electro)catalysts for nitrogen reduction to ammonia (NH_3) under ambient conditions. *Energy Environ. Sci.* 11, 45–56. doi:10.1039/c7ee02220d

Han, D., Liu, X., Cai, J., Xie, Y., Niu, S., Wu, Y., et al. (2021). Superior surface electron energy level endows WP_2 nanowire arrays with N2 fixation functions. *J. Energy Chem.* 59, 55–62. doi:10.1016/j.jechem.2020.11.006

Han, J., Ji, X., Ren, X., Cui, G., Li, L., Xie, F., et al. (2018). MoO_3 nanosheets for efficient electrocatalytic N_2 fixation to NH_3. *J. Mat. Chem. A* 6, 12974–12977. doi:10.1039/c8ta03974g

Jin, H., Li, L., Liu, X., Tang, C., Xu, W., Chen, S., et al. (2019). Nitrogen vacancies on 2D layered W_2N_3: A stable and efficient active site for nitrogen reduction reaction. *Adv. Mat.* 31, 1902709. doi:10.1002/adma.201902709

Kyriakou, V., Garagounis, I., Vourros, A., Vasileiou, E., and Stoukides, M. (2020). An electrochemical haber-bosch process. *Joule* 4, 142–158. doi:10.1016/j.joule.2019.10.006

Li, X., Ren, X., Liu, X., Zhao, J., Sun, X., Zhang, Y., et al. (2019). A MoS_2 nanosheet-reduced graphene oxide hybrid: An efficient electrocatalyst for electrocatalytic N_2 reduction to NH_3 under ambient conditions. *J. Mat. Chem. A* 7, 2524–2528. doi:10.1039/c8ta10433f

Lin, G., Li, H., and Xie, K. (2022). Identifying and engineering active sites at the surface of porous single-crystalline oxide monoliths to enhance catalytic activity and stability. *CCS Chem.* 4, 1441–1451. doi:10.31635/ccschem.021.202000740

Lin, G., Li, H., and Xie, K. (2020). Twisted surfaces in porous single crystals to deliver enhanced catalytic activity and stability. *Angew. Chem. Int. Ed.* 59, 16440–16444. doi:10.1002/anie.202006299

Liu, G., Cui, Z., Han, M., Zhang, S., Zhao, C., Chen, C., et al. (2019). Ambient electrosynthesis of ammonia on a core–shell-structured Au@CeO_2 catalyst: Contribution of oxygen vacancies in CeO_2. *Chem. Eur. J.* 25, 5904–5911. doi:10.1002/chem.201806377

Liu, J., Tang, S., Lu, Y., Cai, G., Liang, S., Wang, W., et al. (2013). Synthesis of Mo_2N nanolayer coated MoO_2 hollow nanostructures as high-performance anode materials for lithium-ion batteries. *Energy Environ. Sci.* 6, 2691–2697. doi:10.1039/c3ee41006d

Lu, Z., Zhou, G., Li, B., Xu, Y., Wang, P., Yan, H., et al. (2022). Heterotopic reaction strategy for enhancing selective reduction and synergistic oxidation ability through trapping Cr (VI) into specific reaction site: A stable and self-cleaning ion imprinted CdS/htnw photocatalytic membrane. *Appl. Catal. B Environ.* 301, 120787. doi:10.1016/j.apcatb.2021.120787

Nazemi, M., Panikkanvalappil, S. R., and El-Sayed, M. A. (2018). Enhancing the rate of electrochemical nitrogen reduction reaction for ammonia synthesis under ambient conditions using hollow gold nanocages. *Nano Energy* 49, 316–323. doi:10.1016/j.nanoen.2018.04.039

Ou, P., Zhou, X., Meng, F., Chen, C., Chen, Y., and Song, J. (2019). Single molybdenum center supported on N-doped black phosphorus as an efficient electrocatalyst for nitrogen fixation. *Nanoscale* 11, 13600–13611. doi:10.1039/c9nr02586c

Ozkan, U. S., Zhang, L., and Clark, P. A. (1997). Performance and postreaction characterization of γ-Mo_2N catalysts in simultaneous hydrodesulfurization and hydrodenitrogenation reactions. *J. Catal.* 172, 294–306. doi:10.1006/jcat.1997.1873

Ren, X., Cui, G., Chen, L., Xie, F., Wei, Q., Tian, Z., et al. (2018). Electrochemical N_2 fixation to NH_3 under ambient conditions: Mo2N nanorod as a highly efficient and selective catalyst. *Chem. Commun.* 54, 8474–8477. doi:10.1039/c8cc03627f

Service, R. F. (2014). New recipe produces ammonia from air, water, and sunlight. *Science* 80345, 610. doi:10.1126/science.345.6197.610

She, Z. W., Kibsgaard, J., Dickens, C. F., Chorkendorff, I., Nørskov, J. K., and Jaramillo, T. F. (2017). Combining theory and experiment in electrocatalysis: Insights into materials design. *Science* 80, eaad4998. doi:10.1126/science.aad4998

Sun, S., Li, X., Wang, W., Zhang, L., and Sun, X. (2017). Photocatalytic robust solar energy reduction of dinitrogen to ammonia on ultrathin MoS_2. *Appl. Catal. B Environ.* 200, 323–329. doi:10.1016/j.apcatb.2016.07.025

Tao, H., Choi, C., Ding, L. X., Jiang, Z., Han, Z., Jia, M., et al. (2019). Nitrogen fixation by Ru single-atom electrocatalytic reduction. *Chem* 5, 204–214. doi:10.1016/j.chempr.2018.10.007

Van Der Ham, C. J. M., Koper, M. T. M., and Hetterscheid, D. G. H. (2014). Challenges in reduction of dinitrogen by proton and electron transfer. *Chem. Soc. Rev.* 43, 5183–5191. doi:10.1039/c4cs00085d

Wickramasinghe, L. A., Ogawa, T., Schrock, R. R., and Müller, P. (2017). Reduction of dinitrogen to ammonia catalyzed by molybdenum diamido complexes. *J. Am. Chem. Soc.* 139, 9132–9135. doi:10.1021/jacs.7b04800

Wu, D., Wang, Y., Ma, N., Cao, K., Zhang, W., Chen, J., et al. (2019). Single-crystal-like ZnO mesoporous spheres derived from metal organic framework delivering high electron mobility for enhanced energy conversion and storage performances. *Electrochim. Acta* 305, 474–483. doi:10.1016/j.electacta.2019.03.077

Xiao, Y., and Xie, K. (2022). Active exsolved metal–oxide interfaces in porous single-crystalline ceria monoliths for efficient and durable CH_4/CO_2 reforming. *Angew. Chem. Int. Ed. Engl.* 61, e202113079. doi:10.1002/anie.202113079

Yang, D., Chen, T., and Wang, Z. (2017). Electrochemical reduction of aqueous nitrogen (N2) at a low overpotential on (110)-oriented Mo nanofilm. *J. Mat. Chem. A* 5, 18967–18971. doi:10.1039/c7ta06139k

Yoon, S., Jung, K. N., Jin, C. S., and Shin, K. H. (2012). Synthesis of nitrided MoO_2 and its application as anode materials for lithium-ion batteries. *J. Alloys Compd.* 536, 179–183. doi:10.1016/j.jallcom.2012.04.116

Zhang, F., Xi, S., Lin, G., Hu, X., Lou, X. W., David)and Xie, K. (2019). Metallic porous iron nitride and tantalum nitride single crystals with enhanced electrocatalysis performance. *Adv. Mat.* 31, 1806552. doi:10.1002/adma.201806552

Zhang, L., Ji, X., Ren, X., Luo, Y., Shi, X., Asiri, A. M., et al. (2018). Efficient electrochemical N_2 reduction to NH_3 on Mon nanosheets Array under ambient conditions. *ACS Sustain. Chem. Eng.* 6, 9550–9554. doi:10.1021/acssuschemeng.8b01438

Zhang, M. Di, Yi, J. D., Huang, Y. B., and Cao, R. (2021). Covalent triazine frameworks-derived N, P dual-doped porous carbons for highly efficient electrochemical reduction of CO_2. *Chin. J. Struc Chem.* 40, 1213–1222. doi:10.14102/j.cnki.0254-5861.2011-3118